CrossMark

Pre-planetary nebulae: a context for principles, progress, and questions on how binaries and magnetic fields produce jets

Eric G. Blackman[1,2]

[1]Department of Physics and Astronomy, University of Rochester
Rochester, NY, 14621, USA
email: eric.blackman@rochester.edu

[2]Laboratory for Laser Energetics, University of Rochester
Rochester, NY, 14623, USA

Abstract. Astrophysical outflows treated initially as spherically symmetric often show evidence for asymmetry once seen at higher resolution. The preponderance of aspherical and multipolar planetary nebulae (PN) and pre-planetary nebulae (PPN) was evident after many observations from the Hubble Space Telescope. Binary interactions have long been thought to be essential for shaping asymmetric PN/PPN, but how? PPN are the more kinematically demanding of the two, and warrant particular focus. I address how progress from observation and theory suggests two broad classes of accretion driven PPN jets: one for wider binaries (PPN-W) where the companion is outside the outer radius of the giant and accretes via Roche lobe overflow, and the other which occurs in the later stages of CE for close binaries (PPN-C). The physics within these scenarios connects to progress and open questions about the role and origin of magnetic fields in the engines and in astrophysical jets more generally.

Keywords. (ISM:) planetary nebulae: general; ISM: jets and outflows; stars: magnetic fields; stars: winds, outflows; stars: AGB and post-AGB; (stars:) binaries (including multiple): close

1. Introduction and overview

Planetary nebulae (PN) are the penultimate evolutionary state of stars below $\sim 8 M_\odot$ (e.g. Balick & Frank 2002) for stars massive enough to evolve off the main sequence during the age of the Universe. They are characterized by an ionization nebula sourced by photons from the hot exposed white dwarf (WD) at their core. Typically, the PN phase lasts of order 10^4 yr after which the remnant WD is left. Planetary nebulae have size scales $\sim 10^{17}$ cm and ages $\sim 10^4$ yr. Pre-Planetary nebulae (PPN) are reflection nebulae typically an order of magnitude smaller and an order of magnitude younger. They are more powerful in mechanical luminosity than PN, and are likely the earlier stage of a PN before sufficient mass clears to expose the ionizing core.

Early models of PN/PPN were based on the spherical interacting stellar wind (ISM) paradigm (Kwok et al. 1978) where a slow wind is followed by a fast wind and the interaction produces a shocked bubble. Evidence of asymmetry and bipolarity emerged later (Feibelman 1985; Gieseking et al. 1985; Miranda & Solf 1990; Lopez et al. 1993). This fostered generalizations of ISW models (GISW) with density asymmetries from equator to pole to explain the asphericity (Balick et al. 1987; Soker & Livio 1989). Basic ingredients of GISW models are present in more modern scenarios and simulations

involving binaries, magnetic fields, and jets (Soker & Rappaport 2000; Blackman et al. 2001; Soker 2002; Balick et al. 2020; García-Segura et al. 2021; Ondratschek et al. 2021).

From the mid 1990s, high resolution HST observations revealed that asymmetry was the rule rather than the exception and the statistical categorization of morphologies became clearer. As a population, PN are overall 80% aspherical, up to 1/2 of the latter exhibiting jets (Balick & Frank 2002; De Marco & Soker 2011). The prevalence of asymmetric PPN among PPN is closer to 100%, with many showing multipolar structure (Borkowski et al. 1997; Sahai & Trauger 1998; Sahai et al. 2009).

The influence of binaries on shaping was proposed from the early days (Paczynski 1976; Soker & Livio 1989; Soker 1994, 1997; Soker & Livio 1994; Reyes-Ruiz & López 1999; Blackman et al. 2001) and is now considered essential to explain the high fraction of asymmetric PN/PPN, particularly when angular momentum (Soker 2006; Nordhaus et al. 2007) and outflow kinematics are considered. While PPN may represent a strongly ($\sim$ few100 yr) collimated jet phase due to close binary interaction, binaries likely also explain the asphericity evolution in the giant stellar wind phases that precede PPN (Decin et al. 2020). In general, binaries induce both equatorial and axial features. Examples of equatorial features include spiral arms and crystalline dust (Edgar et al. 2008; Mauron & Huggins 2006; Kim et al. 2017) and axial features include winds and jets perpendicular to the orbital plane (Hillwig et al. 2016).

Binaries also supply free energy for flows which can amplify magnetic fields (Blackman et al. 2001; Nordhaus et al. 2007; García-Segura et al. 2021; Ondratschek et al. 2021). This amplification may occur in an accretion disk onto a companion, a circumbinary disk, or a merger. The large-scale field that grows can in turn mediate launching and collimation of jets. Magnetic collimation acts to concentrate the pressure of a flow on axis, but the magnetic structures must themselves be collimated by ambient inertial envelopes or tori, as unbounded magnetic structures are unstable.

Observationally, > 200 PN have binaries (Boffin & Jones 2019; Jacoby et al. 2021) and an estimated $\sim 20\%$ of PN are preceded by close enough interaction to have incurred common envelope evolution (CEE) (Miszalski et al. 2009). The number of observed PN/PPN with binaries is less than the 50% fraction for all stars (Miszalski et al. 2009; Raghavan et al. 2010), but this is a lower limit on the prevalence of binary influence. In fact it is plausible that all aspherical PPN/PN are influenced by companions (Ciardullo et al. 1999; Bond 2000; Moe & De Marco 2006; Soker 2006; Corradi 2012; Jones 2020; Decin et al. 2020) including planets (Soker 1996; Reyes-Ruiz & López 1999; Nordhaus & Blackman 2006; De Marco & Soker 2011; Decin et al. 2020; Chamandy et al. 2021), particularly if we allow for the fact that the binary companion may be destroyed by tidal disruption during or after playing a dynamically significant role.

2. Kinematic demands on PPN/PN

PPN warrant special focus because they are kinematically more demanding than PN, and therefore provide stronger limits on source engines if indeed PPN are earlier stages of PN. The difference in kinematic demands is evident in comparing the approximate values for PPN and PN below. PPN fast wind durations are $\Delta t = 100 - 1000$ yr; outflow speeds $v \gtrsim 50$ km/s; mass in nebula $M = 0.5 M_\odot$; mass-loss rate $\dot{M}_f = 5 \times 10^{-4}$ $M_\odot$/yr; momentum injection rate $\Pi \sim 5 \times 10^{39}$ g·cm/s; mechanical luminosity $L_f \geqslant 8 \times 10^{35}$ erg/s. For the PPN slow winds, the corresponding values are $\Delta t = 6 \times 10^3$ yr, $v \sim 20$ km/s; $M = 0.5 M_\odot$; $\dot{M}_f = 10^{-4} M_\odot$/yr; $\Pi \sim 2 \times 10^{29}$ g·cm/s; $L_s \sim 10^{34}$ erg/s.

For comparison, the PN fast wind properties are: $\Delta t = 10^4$ yr, $v \sim 2000$ km/s; $M = 10^{-4} M_\odot$; $\dot{M}_f = 10^{-8} M_\odot$/yr; $\Pi \sim 4 \times 10^{37}$ g·cm/s; $L_f \geqslant 1.3 \times 10^{34}$ erg/s. For the PN slow wind $\Delta t = 10^4$ yr, $v \sim 30$ km/s; $M = 0.1 M_\odot$; $\dot{M}_f = 10^{-5} M_\odot$/yr; $\Pi \sim 6 \times 10^{38}$ g·cm/s; $L_s \sim 3 \times 10^{33}$ erg/s.

Most importantly, for PPN jets where sufficient data has been obtained, mostly all have momenta per unit time satisfying $d\left(Mv_j\right)_{PPN}/dt > 1000L/c > d\left(Mv_j\right)_{PN}/dt > L/c$ (Bujarrabal et al. 2001; Sahai et al. 2009, 2017). Thus, not only do PPN have higher momenta injection rates than the PN, these rates cannot be explained by optically thin radiative driving of jet outflows (Bujarrabal et al. 2001) and thus need another source, most likely involving accretion and close binary interaction (Blackman & Lucchini 2014).

2.1. *Momentum constraints and accretion modes*

The stringent momentum requirements of PPN outflows allow constraining the engine paradigm as follows (Blackman & Lucchini 2014). The mechanical luminosity of all non-relativistic astrophysical jets obey

$$L_m = \frac{1}{2}\dot{M}_{j,N}v_{j,N}^2 \leqslant \frac{1}{2}\frac{GM_a}{\dot{M}_a}r_{in} = \frac{1}{2}\dot{M}_a v_K^2 \qquad (2.1)$$

where $\dot{M}_{j,N}$ is the "naked" jet mass ejection rate, $v_{J,N} \equiv Qv_K(r_{in})$, is the "naked" jet launch speed, $v_K = (GM_a/r_{in})^{1/2}$ is the Keplerian speed at the inner radius r_{in} of the assumed accretor, Q is a dimensionless number with a typical range $5 \gtrsim Q \gtrsim 1$ in MHD jet models (e.g. Blandford & Payne 1982; Pelletier & Pudritz 1992), and $\dot{M}_a$ is the accretion rate. Inequality (2.1) and the definition of Q imply

$$\dot{M}_a > Q^2 \dot{M}_{j,N}. \qquad (2.2)$$

As the jet runs into surrounding material, momentum conservation implies $\dot{M}_{j,N}Qv_k = \dot{M}_{j,obs}v_{j,obs}$, where $\dot{M}_{j,obs}$, and $v_{j,obs}$ are the observed jet mass ejection rate and speed that account for mass pileup. Solving for $\dot{M}_{j,N}$, and plugging into inequality (2.2) allows us to obtain a minimum for $\dot{M}_{j,N}$ and thus $\dot{M}_a$ given by

$$\dot{M}_a > Q^2\frac{\dot{M}_{j,N}}{t_a} \simeq Q\frac{M_{j,obs}v_{j,obs}}{v_K t_a}, \qquad (2.3)$$

where $M_{j,obs}$, $v_{j,obs}$ and t_a are the observed mass, speed and lifetime measured from observations. Numerically we have

$$\dot{M}_a \geqslant 1.4 \times 10^{-4}\frac{M_\odot}{\text{yr}}\left(\frac{Q}{3}\right)\left(\frac{M_a}{M_\odot}\right)^{-1/2}\left(\frac{r_{in}}{R_\odot}\right)^{1/2}\left(\frac{M_{j,obs}}{0.1M_\odot}\right)\left(\frac{v_{j,obs}}{100\text{km/s}}\right)\left(\frac{t_{ac}}{500\text{yr}}\right)^{-1}. \qquad (2.4)$$

So which modes of accretion satisfy this constraint? The values for a number of accretion modes together with the requirements for specific PPN are shown in Figure 1. Bondi-Hoyle-Lyttleton (BHL) onto secondary does not work because typical values would be $\dot{M}_{BH} = 1.15 \times 10^{-6}\dot{M}/\text{yr}$ (Huarte-Espinosa et al. 2013), for a primary wind of mass-loss rate $\dot{M}_W = 10^{-6}M_\odot/\text{yr}$, wind speed $v_W = 10$ km/s, primary mass $M_p = 1.5M_\odot$ and secondary mass $M_s = M_\odot$. Wind Roche lobe overflow (WRLOF) (Mohamed & Podsiadlowski 2012; Chen et al. 2017, 2018) also does not work for a typical separation $a \simeq 20$AU, dust acceleration radius $R_d \simeq 6R_p \simeq 10$AU, primary Roche lobe radius ~ 8.5AU, $\dot{M}_{WR} = 2 \times 10^{-5}M_\odot/\text{yr}$, and component masses $M_s = 0.6M_\odot$ and $M_p = M_\odot$.

The semi-empirically determined accretion rate for the Red Rectangle PPN is $\dot{M}_{RR} \geqslant 5 \times 10^{-5}M_\odot/\text{yr}$, based on the luminosity of the far UV continuum of its HII region (Jura et al. 1997; Witt et al. 2009). This is also too small for most PPN.

There are two classes of accretion modes that do work. First, Roche lobe overflow (RLOF) (Meyer & Meyer-Hofmeister 1983; Ritter 1988) onto the companion from the primary envelope for a companion located outside the giant's envelope. For typical parameters, the RLOF rate is $M_{RL} \simeq \rho_e R_e c_{s,e}^3/(GM_G) \gtrsim 5 \times 10^{-5}M_\odot/\text{yr}$ which is sufficient,

where $\rho_e, R_e, c_{s,e}$ are the density, radius and sound speed of the outer giant envelope, and M_G is its mass.

A second viable accretion mode involves close binary interaction subsequent to when the secondary enters CE. This will only be successful after much of the envelope is unbound as I now explain. Accretion onto the core of the primary (Soker & Livio 1994) or the secondary within CEE can in principle be super-Eddington during the plunge phase of CE before the envelope is unbound, as estimates and simulations suggest $\dot{M}_{CE} \geqslant 10^{-3} M_\odot/\text{yr}$, for secondary and primary masses $M_s = 0.6 M_\odot$ and $M_p = M_\odot$, respectively (Ricker & Taam 2012; Chamandy et al. 2018). But such modes require a "pressure valve" at the engine, otherwise accretion will be halted. Were the accretor a neutron star, neutrinos could supply this valve. For main sequence or WD accretors the jet itself must supply the valve. Estimates of the ram pressure and simulations show that a jet from a main sequence or WD companion during the plunge stage of CE is likely choked within the bound envelope (Lopez-Camara et al. 2021; Zou et al., in preparation). Accretion onto the primary core, or accretion from a shredded low-mass companion (Reyes-Ruiz & López 1999; Blackman et al. 2001; Nordhaus & Blackman 2006) or circumbinary accretion or merger are more effective (Ricker & Taam 2012; García-Segura et al. 2021; Ciolfi 2020; Ondratschek et al. 2021). These all take advantage of the deep gravitational potential well of an accretor and a substantial mass supply. The jet would be visible in the later stages when the CE envelope is unbound. The jet propagates along a reduced density axial channel (Zou et al. 2020; García-Segura et al. 2021; Ondratschek et al. 2021).

2.2. *Energy constraints and time sequence*

Energy constraints on PPN are also revealing. In cases measured, the energy in PPN outflows typically exceeds the envelope binding energy of the AGB host stars and exceeds the orbital energy from inspiral to observed radii from CE (Huggins 2012; Olofsson et al. 2015). This also points to the need for accretion or a merger to tap into the deeper gravitational potential wells.

While PN, unlike PPN, do not strongly constrain the energy or momentum, both PPN and PN do mutually provide a time sequence constraint on the jet and equatorial torus. In different sources, PPN/PN jets are observed to occur both before and after the equatorial dust tori form. In one sample, Huggins (2007) found that PPN jets follow tori by ~ 250 yr on average. That is consistent with equatorial ejecta helping to facilitate collimation, independent of whatever role magnetic fields might play. On the other hand, Tocknell et al. (2014) studied the kinematics of four post-common envelope PN. Three have jets that preceded CE ejection and one has 2 pairs of jets that follow the torus. Although CE is one natural way to get an equatorial torus, a torus may also form from an earlier RLOF phase (MacLeod et al. 2018a) as mass leaves through the L2 point and enters bound orbits.

2.3. *PN are plausibly later stages of accretion driven PPN*

If an accretion-like process onto the core of a companion of mass M_* powers PPN jets, then a connection between PPN and PN is kinematically consistent: the jet mechanical luminosity is

$$L_m \simeq \frac{GM_{*,\odot}\dot{M}_a \epsilon}{2R_i} = 4.5 \times 10^{36} \epsilon_{-1} \left(\frac{M_{*,\odot}\dot{M}_{a,-4}}{R_{i,10}} \right), \tag{2.5}$$

where ϵ_{-1} is a dimensionless efficiency from accretion to jet power in units of 0.1; $M_*, \odot$ is the accretor mass scaled in solar masses; $\dot{M}_{a,-4}$ is the mass accretion rate scaled in units of 10^{-4} M$_\odot$/yr; and $R_{i,10}$ is the inner disk radius in units of 10^{10} cm. The naked

jet speed is

$$v_{j,N} \sim Q v_K \simeq 1600 Q \left(\frac{M_{*,\odot}}{R_{*,10}} \right)^{1/2} \text{km/s},\qquad(2.6)$$

so that the predicted observed PPN jet speed after mass pile-up from momentum conservation when the ejecta are optically thick, is given by

$$v_{j,obs} \simeq \frac{M_f v_f}{f_\Omega M_{env} + M_f} \sim 80 \text{km/s}.\qquad(2.7)$$

But once the outflow transitions to the PN stage the optical depth τ_d to dust scattering drops below unity, as estimated by

$$\tau_d = 2.5 \times 10^{-3} \left(\frac{n_d}{2.5 \times 10^{-13} \text{cm}^{-3}} \right) \left(\frac{\sigma_d}{10^{-8} \text{cm}^2} \right) \left(\frac{R}{10^{18} \text{cm}} \right),\qquad(2.8)$$

where the dust number density n_d and scattering cross section σ_d are scaled to typical PN values. This is a simple explanation for the trend that PN have less power but faster winds. The naked jet, and thus the naked jet speed, is more exposed in PN as the optical depth decreases. More detailed transitions from PPN to PN speeds and powers can be predicted from engine models as a function of age and compared to individual sources or statistical observations.

3. Binary interactions: from weak to strong for low mass giants and low mass companions

Since the mechanisms of accretion that work to power PPN require binary interactions with orbital radii at least small enough for the primary to overflow its Roche lobe, the question of how sufficient numbers of binaries get close enough to produce the required number of PPN/PN arises. Observations suggest that at least 20% of PN have to have incurred CE (Miszalski et al. 2009). But since only 2.5% of PPN/PN should incur CE if tides alone are responsible for orbital decay to the RLOF phase (Madappatt et al. 2016), something else to tighten the orbits is needed.

For wide separations, analytic estimates of BHL accretion, which are too low to power PPN, match simulations and an accretion disk forms around the primary primarily from infall toward the retarded position of the secondary (Huarte-Espinosa et al. 2013; Blackman et al. 2013). But for this mode of accretion, such a high fraction of the mass lost from a typical AGB wind from which the BHL accretion draws, leaves without interacting much with the secondary. Therefore the orbit tends to increase (Chen et al. 2018; Decin et al. 2020). If however, for somewhat tighter orbits, WRLOF occurs (Mohamed & Podsiadlowski 2012), wind accelerated orbital decay (Chen et al. 2017, 2018) is possible and can greatly increase the number of systems that ultimately incur close enough interactions to produce PPN. More work is needed to make exact predictions.

Figure 2 shows the different consequences of initial binary separation, and where a PPN can be powered.

3.1. *Distinction between "PPN-W" and "PPN-C" and Example Cases*

Two classes of mechanisms work best to power PPN feature in the above discussion. In the symposium talk, I distinguished them as "preceding" and "succeeding" CE. In the discussion with R. Sahai, J. Kluska, and N. Soker afterward, it was suggested to me that a better distinction might be AGB and post-AGB since there are PPN objects which have 100 to 1000 day orbital periods (Bollen et al. 2021) and will never incur CE since their envelopes are mostly gone. However, what I wish to convey in a classification
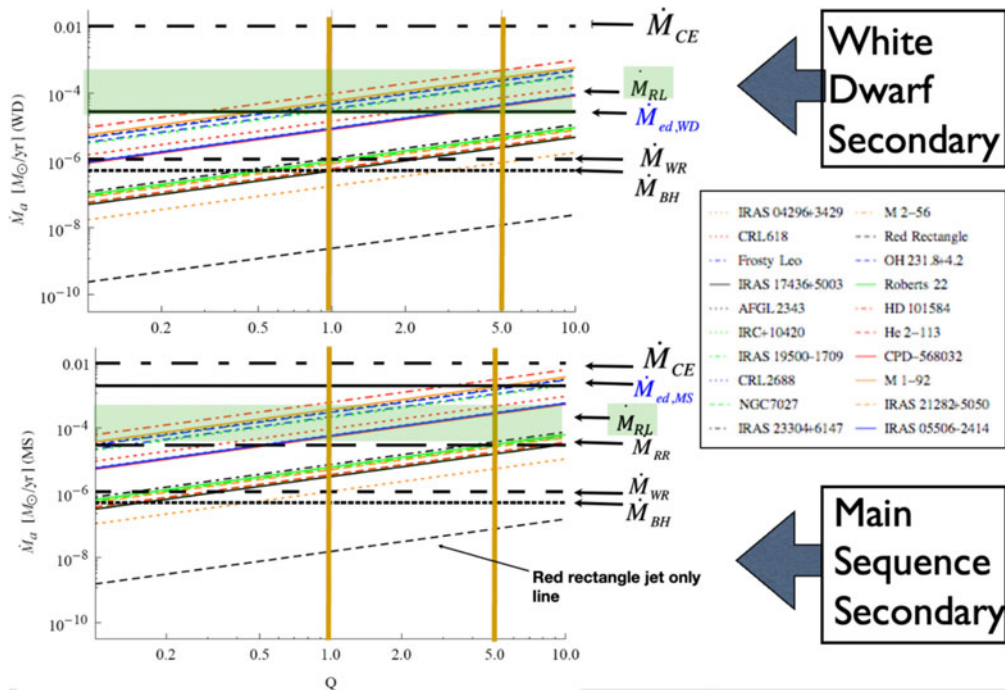
Figure 1. Adapted from Blackman & Lucchini (2014): Horizontal lines in each panel show examples of theoretically estimated accretion rates (BHL M_{BH}; Wind Roche lobe overflow M_{WR}; Red Rectangle based on HII region M_{RR}; Roche lobe overflow M_{RL}; Eddington M_{ed}; Accretion deep in common envelope M_{CE}) and the diagonal lines correspond to momentum requirements inferred from observations for each of the objects in the table as Q, the ratio of naked jet speed to Keplerian speed at the disk inner radius, is varied. The vertical gold lines bound the typical range of Q from MHD jet models. The accretion mode of a given horizontal line is sufficient to power jets only where the points on a given horizontal line lie above those on a given diagonal line. The figure shows that RL and higher accretion rates are sufficient to power PPN but lower accretion rates are not generally sufficient.

scheme is distinguishing PPN mechanisms by their binary separation. This distinction can apply to systems with either AGB or RGB primaries.

Taking all of this into account, I label the two classes as PPN-W and PPN-C, where the W and C stand for "wide" and "close" and correspond, respectively, to orbital separations larger and smaller than the original giant envelope. Thus PPN-W would include RLOF accretion PPN, and PPN-C refers to close binary mechanisms. Inasmuch as the PPN in the aforementioned (Bollen et al. 2021) objects depend on the interaction of the observed binaries, these objects would be classified as PPN-W. I now discuss some specific example objects, and subsequently review some simulations in this context.

Figure 2 shows schematically the binary separation that distinguishes these two PPN classes, and Figure 3 shows two examples. Other examples are discussed below.

3.2. *Example PPN with the PPN-W and PPN-C distinction in mind*

HD 44179: Red Rectangle: The Red Rectangle PPN is best modeled as a main sequence secondary, accreting from the primary giant in an elliptical orbit, and moving in and out of the Roche Lobe of the primary (Witt et al. 2009) and is an example of a PPN-W. The outflow emanates within the central cavity of a cicumbinary torus of thickness 90 au and cavity diameter of 30 au, consistent with the formation of a torus from RLOF
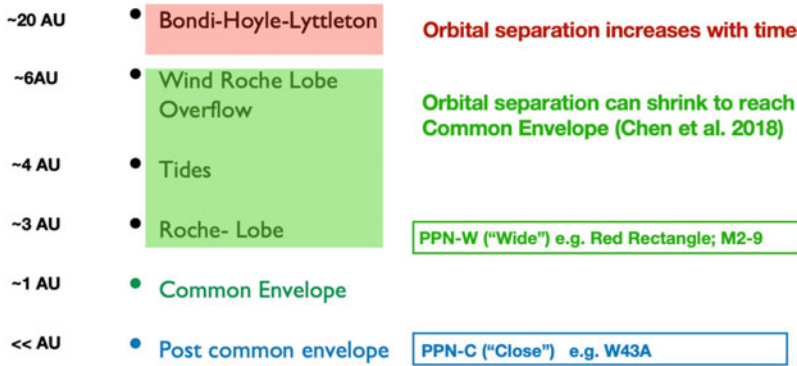
Figure 2. With decreasing orbital separation from top to bottom, the figure schematically indicates that separations that are too wide initially will widen further with BHL accretion. The red shading indicates no PPN will form from these systems. In the green region, indicated by the dominant mechanisms listed, the orbital separation can shrink (Chen et al. 2018). PPN can be produced at two key stages: in the RL regime indicated for this plot around 1-3 au (corresponding to PPN-W) and after much of the envelope is unbound in the post-CE stage (corresponding to PPN-C). Suggested examples of these two cases are shown in Figure 3.

(MacLeod et al. 2018a). The HST composite from Cohen et al. (2004) shows a bipolar axis length of $\sim 1.5 \times 10^4$ au. The jet produces a blue shift in Hα emission, modulating the primary's envelope emission. The accretion rate as constrained by the luminosity needed to source far-UV continuum for its HII region (Jura et al. 1997) assuming a distance of 710 pc, implies a maximum accretion disk temperature of 17,000K and a minimum accretion rate of $\dot{M}_a \geqslant 5 \times 10^{-5} M_{\odot}$/yr. This is is plotted in Figure 1 and is much larger than the constraint purely from the jet momentum calculation above, but can be accommodated by RLOF.

M2-9: M2-9 is a PPN-W with a jet from a companion orbiting in an 88-120 yr period, and injecting the flow into a hot bubble cavity. Early binary scenarios (Soker & Rappaport 2001) are now updated as Corradi et al. (2011) favored a fast jet induced illumination of the inner cavity (Doyle et al. 2000) rather than a photon source, based on delay time between knots. The jet produces mirror symmetry. There has been some ambiguity in interpreting this as potentially a symbiotic (RGB + WD companion instead of AGB+WD/MS) but the distinction is not important from a basic theoretical jet mechanism perspective since accretion from the RGB envelope onto the companion vs. accretion from the AGB envelope onto the companion both represent "W" nebulae in the classification above. Lykou et al. (2011) also identify a "disk/torus" from 15-900 au which may play a role in collimating the flow.

W43A: W43A is one of 15 "water fountain" sources exhibiting water maser emission (Diamond & Nyman 1988; Imai et al. 2002, 2005; Vlemmings et al. 2006; Amiri et al. 2010; Chong et al. 2015). Tafoya et al. (2020) interpreted W43A ALMA data in CO to reveal knots separated by a few years, a jet launched at 175 km/s, decelerating to 130 km/s, and collimated from 90 au to 1600 au. There is no binary detected, but Tafoya et al. (2020) suggest that the knots could indicate the influence of a binary period e.g. an eccentric orbit. That would make this a PPN-W. However, the tight collimation suggests that the outflow is produced from a tighter binary engine, suggesting that it may be a PPN-C outflow. The knots would then indicate a secular time scale (perhaps due to unsteady viscous accretion) compared to the much shorter orbital time scale at the base of the jet.

García-Segura et al. (2021) also argued that W43A is a post-CE object, also making it a PPN-C. In fact Khouri et al. (2021) observed that W43A and the other 14 known water fountain sources all likely incurred CEE, which implies that they are all PPN-C.

Magnetic fields measured in W43A are 85 mG at ~ 500 AU and are strong enough to collimate the measured outflow on those scales (Vlemmings et al. 2006; Amiri et al. 2010). These fields are quite far from the likely jet origin, but if scaled even linearly down to 10^{11} cm could provide the $> kG$ fields needed to be dynamically significant at the engine. Whether the source of the fields at 500 au is separate from, or an extension of, the fields generated in the jet engine is not yet clear.

IRAS16342-3814: This is another water maser fountain source with a collimated molecular jet and dust emission (Murakawa & Izumiura 2012; Sahai et al. 2017). As observed by Sahai et al. (2017), its high-speed jet exhibits 5 knots/blobs in each lobe, and gas of density $\sim 10^6/\mathrm{cm}^3$ is expanding in a 1300 au torus. There has been a rapid increase of mass-loss rate to $> 3.5 \times 10^{-4} M_\odot/\mathrm{yr}$ in the past ~ 455 years which suggests CEE.

Sahai et al. (2017) also constrain the circumstellar component ages for the AGB circumstellar envelope (~ 455 yr); extended high velocity outflow (EHVO) (130 to 305 yr with speed ~ 500 km/s); dust torus (160 yr); high velocity outflow (HVO) (~ 110 yr, with speed ~ 250 km/s). These indicate that the torus emerges several hundred years after the rapid AGB mass-loss increase, and the HVO appears very soon after torus formation. This is consistent with the time sequence in the Huggins (2012) sample mentioned earlier.

Although data from this object are not used in Figure 1, the inferred kinematics also require accretion rates as high as RLOF from the primary, or accretion operating within/after CEE. The high collimation, the absence of a detectable binary and the presence of a substantially increased AGB envelope all point to this source being classified as a PPN-C.

Calabash (Rotten Egg) Nebula OH232.84+4.22:

This object has a binary engine consisting of a Mira (AGB) variable (Cohen et al. 1981; Kastner et al. 1998), and an A0 main sequence companion in a likely $\geqslant 50$ au orbit (Sánchez Contreras et al. 2004). The orbit is too wide to provide the needed accretion rate ($\sim 10^{-4} M_\odot/\mathrm{yr}$) to power the ~ 0.2 pc bipolar nebular lobes and explain the rate at which $\sim 1 M_\odot$ of circumstellar molecular gas from previous mass loss arose. Sánchez Contreras et al. (2004) speculate that an FU Orionis type outburst from accretion onto the companion might account for this. The source would then be a PPN-W.

However, another possibility is that there was a previous binary inspiral via CE which ejected envelope material and powered the PPN as a PPN-C. The outflow could then be sourced by circumbinary accretion or the release of free energy due to pre-merger core activity, with energy released as heating or mediated by self-generated magnetic fields along the lines of Ondratschek et al. (2021) discussed below. In this case, the presently observed wide binary would have little to do with what actually produces the collimated outflow. The Calibash nebula also has a rather collimated spine with little wobble. Sabin et al. (2015), using CARMA, found polarization that indicates a mostly toroidal ordered magnetic field perpendicular to the outflow. This is consistent with the orientation expected if some magnetic collimation were at work.

Dodson et al. (2018) found that H_2O maser emission aligned along bipolar lobes is perpendicular to an SiO maser disk and is ~ 40 yr old, confirming that mass loss is ongoing in the jet and that the history of mass loss is unsteady.

4. Common Envelope Evolution

CEE begins when the giant envelope engulfs the orbit of the secondary and the latter plunges in. The envelope could directly engulf the companion upon expansion to a giant phase for initially small enough orbital radii, but for most systems that incur CE, the
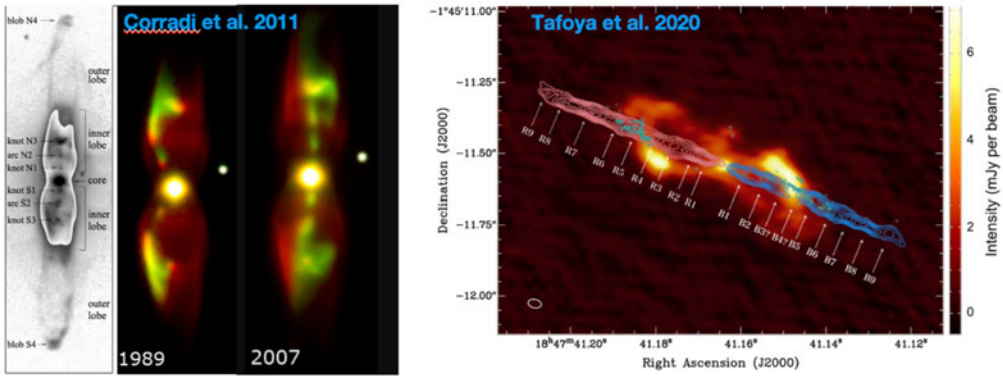
Figure 3. Left panel shows images of M2-9 from Corradi et al. (2011) and right panel shows W43A from Tafoya et al. (2020). M2-9 is likely a PPN-W, as the jet is produced from an accreting companion just outside the orbital radius of the giant, and consistent with RLOF accretion. Mirror symmetry is seen as the jet orbits and illuminates the surrounding bubble. In contrast, W43A is more likely a PPN-C, having a tightly collimated straight jet, plausibly produced deep within an CE, after a companion plunged close to the primary core.

process is likely preceded by a slow inward orbital migration that proceeds from wind induced orbital decay, tides, and RLOF. As discussed earlier, although the binaries that undergo BHL accretion expand because so little of the mass lost from the primary interacts with the secondary, closer binaries that incur stronger interaction via WRLOF can tighten. This tightening is further exacerbated by tides. CEE is ultimately important both for determining the properties and structure of mass loss as well as the orbital evolution of stellar systems that may include planets. The resulting effect on binary evolution and the efficacy with which angular momentum is removed from the system influences compact object merger rates and basic phenomenological properties of both high and low mass stellar systems (Paczynski 1976; Iben & Livio 1993; Taam & Sandquist 2000; Ivanova 2011; Ivanova et al. 2013a,b; Postnov & Yungelson 2014).

CEE is challenging to model accurately because of the wide range of temporal, spatial, and density scales from the 1 au envelope radius to the core dynamics $\leqslant 10^{10}$ cm, let alone the nebular outflow extending out to $\geqslant 0.1$ pc if one is to follow the full influence of CEE from giant star to PN. CE simulation efforts have, however, been progressing with substantial progress (Ricker & Taam 2012; Ivanova et al. 2013a,b, 2015; Ivanova & Nandez 2016; Ivanova 2018; Ohlmann et al. 2016a,b, 2017; MacLeod & Ramirez-Ruiz 2015a,b; MacLeod et al. 2017, 2018a,b; Staff et al. 2016a,b; Iaconi et al. 2017, 2018, 2019, 2020; Chamandy et al. 2018, 2019a,b, 2020, 2021; Ondratschek et al. 2021). Most simulations are run for ~ 100 days with the long end being ~ 4500 days (Ondratschek et al. 2021). Even that however, is short compared to the 100 to 1000 yr lifetimes of PPN, and the $\sim 10^4$ yr lifetimes of PN.

Important open questions include: how efficiently can a companion of given mass unbind the envelope upon inspiral? Does unbinding require recombination energy (Soker 2004; Ivanova & Nandez 2016; Glanz & Perets 2018)? What is the effect of convection? Convection might reduce the efficiency with which recombination might supply energy (Wilson & Nordhaus 2019) but might also redistribute energy more efficiently causing more mass to be unbound (Chamandy et al. 2018). For simulations without convection and without recombination however, CE may unbind the AGB envelope if the results from runs of 260 days for a $1.8M_\odot$ primary and $1M_\odot$ secondary were extrapolated to ~ 7 years (Chamandy et al. 2020), as shown in Figure 4.
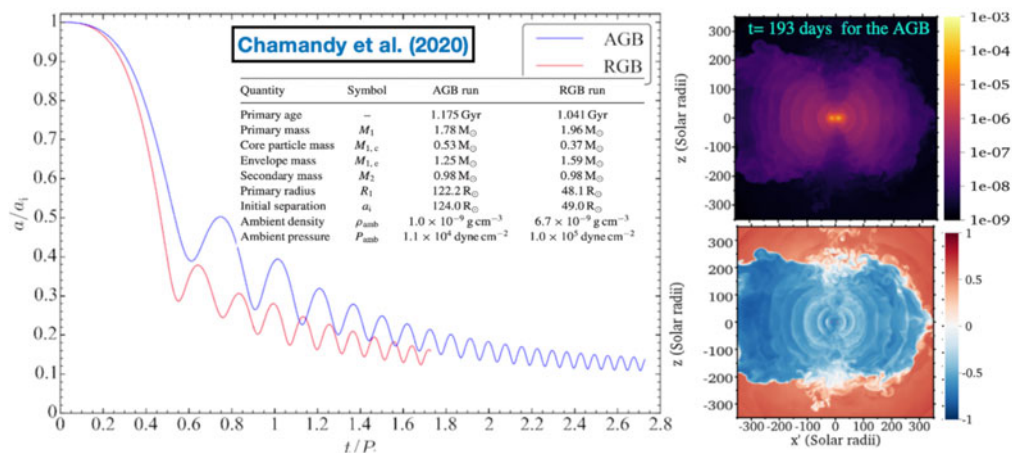
Figure 4. taken from Chamandy et al. (2020). Left panel: inter-particle separation for AGB and RGB runs with the rapid plunge phase, followed by slow inspiral. Time is normalized by orbital period: 96.5 days for the AGB curve and 23.2 days for the RGB. Separation is normalized by the initial orbital separation: 124 $R_\odot$ for AGB and 49 $R_\odot$ for the RGB. The AGB run is shown to ~ 260 days. The rate of unbinding at the end is steady at $0.17 M_\odot/$yr, and would unbind the full envelope within 7 yr if extrapolated. Right panel: vertical slices through the orbital plane of the AGB at $t = 193$ days for the AGB run. The left slice is the gas density in g/cm^3 and the right slice indicates bound (blue) and unbound (red) gas at this time quantified by a dimensionless measure ranging from 1 (strongly unbound) and -1 (strongly bound.

Armitage & Livio (2000) and Chevalier (2012) examined the ejection of CE by jets launched from a neutron star that inspirals inside the giant envelope. Others have considered different companions (Soker 2004; Papish et al. 2015; Soker 2015, 2016; Moreno Méndez et al. 2017; Shiber et al. 2017; Shiber & Soker 2018; Shiber et al. 2019; López-Cámara et al. 2019; Lopez-Camara et al. 2021). As discussed earlier, accretion onto a plunging main sequence or WD companion before the envelope is unbound, requires a pressure release valve in order to prevent thermal pressure from building up and abating the accretion (Chamandy et al. 2018). Jets from MS and WD companions are largely choked by the bound envelope after plunge-in for reasonable jet powers (Lopez-Camara et al. 2021). This can be estimated by comparing the ram pressure of the jet with the thermal pressure of the envelope. The total energy injected by the jet $L_m t_j$ where t_j is the jet lifetime, can also be compared with the binding energy to identify a minimum time scale over which this outflow could unbind the envelope, compared to other unbinding mechanisms. The efficiency with which the jet energy is used to unbind mass can also be studied in simulations. Although the jet may appear to be unimportant in a short simulation, over longer times its effect may be significant (Zou et al., in preparation).

Even if the jet starts during RLOF before the secondary plunges, it will be connected by an accretion stream to the envelope which will facilitate an already rapid drag-in to inspiral. Thus it seems unlikely that a jet would produce much unbound mass before plunge in. For a limited set of binary parameters which includes the case of a 1 au primary of mass 18 $M_\odot$ and a 5.4 $M_\odot$ secondary with no jet, MacLeod et al. (2018b) found that RLOF can last decades but that once the secondary enters the envelope the plunge is rapid. There have not yet been numerical studies that include accretion from the envelope and include a jet such that the envelope mass, accretion stream, and orbital inspiral are all self-consistently included, but the lessons learned so far do not suggest that the jet could prevent inspiral.

For CE, the list of topics with opportunity for more work includes: (i) the inclusion of convection; (ii) more complete treatments of the equation of state and better approximations to inclusion of recombination energy; (iii) more detailed radiative transfer; (iv) studying the sensitivity to initial conditions and initial binary separation; (v) increasing the duration of simulations; (vi) limiting the effects of softening of potential wells by smoothing and limited numerical resolution; (viii) ensuring conservation of energy and angular momentum in long term simulations.

5. Role of Magnetic Fields in Driving and Shaping

Because collimated jets from MS and WD companions are substantially choked during CEE plunge-in as described above, jets that produce PPN would be most likely visible either in the (i) RLOF phase before plunge producing a PPN-W or (ii) after substantial CE ejection has occurred producing a PPN-C.

So what about the collimation in each of these cases? Magnetic fields are likely important for jet launch and tight collimation as toroidal hoop stress can act to concentrate the pressure of the flow to an axial spine. But all magnetically collimated flows still require ambient pressure for stability. In fact there is no astrophysical context with a collimated jet for which an ambient wind or thermal pressure surrounding the jet is ruled out. In the present context, CE provides tori for inertial collimation both in the RLOF phase (MacLeod et al. 2018a,b) and in the post-CE ejection phase. We discuss the latter here.

García-Segura et al. (2018), ran 2-D simulations for $10,000$ yr, starting at 1 au with output from CEE simulation of Ricker & Taam (2012) at a time of 47 days as the initial conditions. Zou et al. (2020) ran 3-D simulations for 10,000 days, starting at 100 au with output from the CEE simulation of Reichardt et al. (2019). The results from both of these simulations exemplify the basic principle that a uncollimated hydrodynamic wind injected within the output of a CE simulation can be collimated by the ejecta. However the outflow of García-Segura et al. (2018) does not remain collimated and instead transitions to a wide barrel/elliptical structure in the absence of magnetic fields.

Importantly, magnetic fields are a "drive belt" not a "motor" and require a source of free energy (convection, orbital, accretion) supplied by binary interactions. Magnetic fields and binaries are therefore not competing mechanisms, but operate in symbiosis. The binary supplies the free energy and sets up the environment within which the magnetic field is amplified and functional. Analytic estimates for dynamically important disk engine field strengths in the PPN context give values $\geqslant 10$ kG (Blackman et al. 2001).

Most astrophysical MHD jet simulations have separated the detailed origin of the magnetic fields from the outflow dynamics. For example, the surface of the anchoring rotator has often been treated as boundary conditions with an imposed field. But progress is emerging across astrophysical disciplines in unifying field origin and jet formation self-consistently (Kathirgamaraju et al. 2019; Ruiz et al. 2021; Ondratschek et al. 2021). The range of approaches to the problem in the PPN/PN context has included analytic calculations (Pascoli 1997; Blackman et al. 2001; Tout & Regos 2003; Nordhaus & Blackman 2006; Nordhaus et al. 2007) focused on dynamo and/or power generation and three types of numerical approaches discussed in the subsections below.

5.1. *Shaping from imposed dynamically important magnetic fields*

Shaping of flows with an imposed magnetic field has been a long standing approach to model some aspects of outflow shaping (Chevalier & Luo 1994; Garcia-Segura 1997; García-Segura et al. 1999, 2005; Balick et al. 2020). Balick et al. (2020), for example, imposed a flow of 400 km/s with opening angle 40 deg injected normal to a sphere of radius 1000 au. A toroidal field was imposed with initial values varying between $0.003 \text{G} \leqslant$

$B \leqslant 0.3$G. The framework was tuned to produce resultant angular distributions of speeds and outflow geometry consistent with e.g. OH231.8+04.2 (Alcolea et al. 2001; Sánchez Contreras et al. 2018) and CRL618 (Balick et al. 2013; Riera et al. 2014) Hen2-104 (Corradi et al. 2001) and MyCn18 (Bryce et al. 1997; O'Connor et al. 2000).

Although such a method does not self-consistently generate jets because a strong magnetic field is imposed as an initial condition, one can still use the results to match observations and then infer what the field strength and geometry should be to inform further observations and theory. The method has not been used to study the possible differences between PPN-C and PPN-W which would would be valuable.

The next subsections focus on more steps toward self-consistent generation of collimated outflows, specifically in the PPN-C context.

5.2. *Multi-stage 2-D MHD simulations*

A second approach is to use output from 3-D CE simulations to set initial conditions for 2-D simulations, with only an imposed weak seed field. The weak field may grow dynamically and produce self-generated MHD outflows. Using this approach, García-Segura et al. (2020, 2021) started with the conditions of the Ricker & Taam (2012) CE after 56.7 days at which point 25% of the envelope is unbound and mass is being lost at the high rate of $2M_\odot/$yr. A weak seed magnetic field with toroidal and poloidal components was imposed on the scale of 1 au. The field grows, causes angular momentum loss, disk collapse, and a magneto-centrifugally launched wind. After 120 days, they took output for a second 2-D simulation, this time using an expanding grid envelope. They evolve the result for > 1000 years. They find that the resultant CE outflow forms from a circumbinary disk and a very tightly collimated outflow whose properties plausibly resemble W43A and the Calabash nebula. This computational model produces a PPN-C in the aforementioned classification scheme. The jet is produced after much of the envelope is ejected and the binary orbit is 7 times smaller than the RGB envelope at the time of the conditions used from Ricker & Taam (2012).

This approach is a step toward more self-consistency in that the imposed magnetic field is weak and the outflow is self-generated. There are certainly limitations to the fidelity of 2-D and the expanding grid, but the 2-D simulations can be run for > 1000yr which is orders of magnitude longer than what can be expected for 3-D simulations. There are always trade-offs, and precise realism is not always necessary to gain some insight.

5.3. *Simulations with "organic" 3-D magnetic field amplification and jet formation*

Complete modeling of a PPN-W formation requires simulating an RGB or AGB in RLOF with a companion accretor, and allowing the field to amplify within the accretion flow. A self-consistent magnetically mediated outflow should grow, along with any circumbinary molecular torus that might aid in collimation. For self-consistent PPN-C formation, a simulation would instead require the full CEE after the RLOF phase, starting with a stellar seed magnetic field in the giant and computing how the combination of CE, inspiral, field amplification, outflow, and collimation subsequently proceed.

There has not yet been a fully self-consistent simulation of a PPN-W by the above standard, and so here I focus on PPN-C. Indeed, Ondratschek et al. (2021) have broken new ground for the study of PPN-C with a full MHD CEE simulation that shows organic growth of a jet mediating magnetic field and collimated outflow production in 3-D. They use the AREPO code and include a prescription for recombination energy, which is important as it causes the simulated envelope to become unbound during the jet evolution. They start with a weak dynamically insignificant seed magnetic dipole field

in the AGB star of mass 0.97 $M_\odot$ and include a companion of 0.243 $M_\odot$ as fiducial run. This mass ratio is then $q = 0.25$, but they also carried out runs for $q = 0.5$ and $q = 0.75$ that produced qualitatively similar results. They track the inspiral to ~ 4000 days.

The magnetic field is amplified some 15 orders of magnitude on the time scale of the simulations. Comparing runs with and without a magnetic field, they find that the field makes little difference to unbinding after 1000 days (also true of semi-analytical dynamos, Nordhaus et al.2007), which is expected: as discussed above, the magnetic field is not an extra source of energy but draws its energy from the sources already there, the orbital energy in this case. The field amplification arises from some combination of shear, and turbulence sourced by some combination of MRI, and Kelvin-Helmholtz instability and the emergent jet launches with cross sectional diameter of the circumbinary disk engine. The exact analytical modeling of the system has yet to be carried out, but this clearly demonstrates a type of PPN-C outflow, as the jet emanates from a circumbinary region which is a factor of ~ 8 times smaller than the initial AGB stellar radius. The most important lesson that this simulation highlights, is that the magnetic field facilitates formation of a magnetically driven and strongly collimated jet along a narrow axial channel. The collimated jet is absent without the field.

The simulation by Ondratschek et al. (2021) is a substantial step toward high fidelity global simulations of PPN-C. Under the hood, there are a number of issues that warrant further work and discussion. Convection in the AGB star has not been included. The treatment of recombination is approximate and non-local, and the extent to how this interfaces with convection is relevant in the broader CE context as discussed earlier. Convection will also add a disordered component to the initial seed dipole field and so the extent to which it influences the overall magnetic launch and collimation is also important. In the presence of convection, even the seed field may require a dynamo in the star since exponential generation is needed to compete with turbulent diffusion. There is also the question as to the relative role of a magnetic tower or a magneto-centrifugal launch, a distinction discussed further in the next section.

5.4. *Magnetic Tower, Magneto-centrifugal Launch, or Magnetic Bomb?*

Magnetically mediated launches that depend on the presence of large-scale magnetic fields are not all the same. There are essentially three types as described below. Although all share the fact that a gradient in toroidal field magnetic pressure helps to propel material and the hoop stress helps to collimate, they also differ in key aspects. They may not be mutually exclusive in a given source. For example, a magnetic tower may be embedded within a broader magneto-centrifugal launch, however, we do not yet know which mechanism dominates in any given source.

The magnetic tower (MT) (e.g. Lynden-Bell 1996, 2003; Uzdensky & MacFadyen 2006; Gan et al. 2017) can be initiated from magnetic field loops anchored between footpoints in relative differential rotation, for example loops that link a stellar core to a surrounding torus. The footpoint separation may be of comparable scale to the radius at which they are anchored, but both footpoints are contained in the engine itself. The differential rotation winds up the field, creating a toroidal component that establishes a magnetic pressure force which pushes material upward. The hoop stress collimates the pressure of this rising tower, but only when the ambient medium is surrounded by a balancing ambient pressure. The magnetic field is parallel to the axial flow on the jet axis, and becomes increasingly toroidal away from the axis toward the jet boundary. The outflows can remain marginally magnetically dominated inside the jet out to observable scales within the tower and maybe out to arbitrarily large-scales. Importantly, both signs of magnetic flux are contained within the structure that would appear as the jet tower

because both of the original loops are within the jet. Their separation defines the diameter at the base of the tower. The jet contains zero vertical net magnetic flux.

The magneto-centrifugal launch (MCL) (Blandford & Payne 1982; Pelletier & Pudritz 1992) is a more widely invoked class of models for which the starting point is a large-scale open magnetic field with only one anchoring foot-point sign at the engine base and the other foot-point essentially at infinity. Plasma loaded onto quasi-rigid field lines at the base is centrifugally flung along these lines as angular momentum of the base is transferred via the field lines to the plasma. At the Alfvén radius, where the flow energy density becomes comparable to that of the field, the torodial field magnitude is comparable to that of the poloidal field and supplies some outward pressure and collimation. On larger scales farther from the engine, say $\gtrsim 100R_{in}$, the flow kinetic energy marginally dominates field energy within the jet, the opposite of the magnetic tower. Importantly, for the MCL, only one sign of poloidal magnetic flux resides within the jet, also in contrast to magnetic tower. For a source of magnetic field produced in a PPN accretion disk, MCL outflow scalings have been applied to PPN (Blackman et al. 2001). For the MCL like the MT, ambient collimation of the inner magnetic structures by some ambient flow or pressure is also needed and all simulations demonstrating collimation and steady jets have pressure equilibrium at the jet boundary.

One more magnetically mediated outflow model is a magnetic bomb (MB) (Matt et al. 2006). Here a wound magnetic field acts like a capacitor, suddenly releasing its energy in outflows. The starting point is an evolved star for which differential rotation has been established between the collapsed degenerate core, and the expanded envelope. The initial field anchored at the core be open, as per the MCL. However, this field can be weak initially, and there is no need to load mass from the core onto the field lines as the field is already mass loaded. Differential rotation between the envelope and core winds up the toroidal field. After the field reaches some threshold, it rapidly drives polar outflows from vertical magnetic pressure gradients, and equatorial outflows as the wound field in each hemisphere also squeezes flow outward from the equator. Like the MT, differential rotation is important from the start, but the primary differential rotation for the MB is vertical not radial. The MB for an initial dipole field would have just one sign of magnetic flux in the outflow, similar to the MCL and distinct from the MT.

5.5. *Measured Magnetic Fields*

Given the importance of magnetic fields, some further comments on what has been measured warrants mention. The measurement of magnetic fields in W43A (Vlemmings et al. 2006; Amiri et al. 2010) and the evidence for toroidal fields in the Calibash from polarization (Sabin et al. 2015) were mentioned above. Fields have also been measured in other AGB stars via masers (Herpin et al. 2006), masers in the OH shell of NML Cygni Etoka & Diamond (2004), and in Miras (Kemball & Diamond 1997; Kemball et al. 2009). Synchrotron emission in the post AGB star IRAS 15445-5449 has been measured at 7000 au, indicating a mG field which could collimate the jet (Perez-Sanchez et al. 2013). Leone et al. (2014) found no evidence for $>$ kG fields in the central stars of PN, but a field of $B \sim 655$G in NGC4361.

However, an important point is that none of the above measurements probe the field on the jet "launch" scales (< 0.01 au). Instead, they are measurements of the jet "propagation" (> 1 au) scales. That fields are dynamically important on propagation scales is important, but these do not directly constrain the jet formation at its engine.

Also, distinguishing the MT from MCL cannot be done with polarization measurements because they are ambiguous to 180 degrees in field orientation. Measurements

that constrain whether the sign of the flux is uniform across the jet in a given (indicating MCL or MB) hemisphere or has two reversals across the jet (indicating MT) are needed.

6. Persistent challenges and distinguishing PPN-C from PPN-W

While PPN and CEE are likely associated, one challenge is to identify direct signatures of a CEE event (Khouri et al. 2021) and possibly to associate the two more directly. There remain some challenges that come with comparing theory, simulation and observation both in terms of the limits of numerical simulations and in predicting distinguishing features of PPN-C and PPN-W.

6.1. *Convection, magnetic fields, and the limits of numerical simulations*

In addition to potentially delocalising the deposition of recombination energy discussed earlier, convection also leads to turbulent diffusion of large-scale magnetic flux. In turbulent astrophysical systems, large-scale flux is almost never frozen. (Think of the Sun, where the large-scale field reverses every 11 years. This would be impossible if flux were frozen.) This raises the question of the initial field in the giant star used for simulations without convection (e.g. Ondratschek et al. 2021). In reality, the stellar field would not be exclusively ordered but may even be dominated by a random component. The total field would need to be sustained by large and small scale dynamos to overcome the exponential decay from turbulent diffusion. How various dynamos conspire in these engines to produce the dynamically significant large-scale fields, and how the turbulence affects the level of collimation of the jet remains to be studied.

A second open issue is that large scale transport rather than local isotropic turbulence may dominate in disks, whether or not the magneto-rotational instability (MRI) is the dominant instability (Blackman & Nauman 2015). The fraction of small scale, mesoscale, or large-scale transport is not well constrained. The scale of transport determines where energy is dissipated, which in turn determines the observed spectral signatures of accreting systems. Dissipation that occurs deep within an optically thick disk will produce thermal emission but dissipation that occurs in a corona or jet can be non-thermal. The fraction of thermal versus non-thermal emission can thus be used as a proxy for the scale of angular momentum transport (Blackman & Pessah 2009).

Another pervasive issue, is how sensitive the phenomenological output from simulations is as a function of initial and boundary conditions. Numerical simulations are useful to study small pieces of a physical system at high resolution or "kitchen sink" approaches at low resolution. But for kitchen sink simulations, the question of convergence is substantial. Dynamos and accretion disks are examples for which intermediate fidelity simulations can cause confusion. Suppose, for example, that analytic theory were to predict that in the asymptotic limit of large magnetic Reynolds number, a particular dynamo magnetic growth rate is independent of magnetic Reynolds number. Further suppose that the real astrophysical system of interest has a magnetic Reynolds number much larger than one could ever hope to simulate. If a simulation then exhibits a dependence on magnetic Reynolds number, it is not easy to determine whether the theory is wrong or whether the simulation is not in a sufficiently asymptotic regime to be realistic. In the case of the solar dynamo, intermediate fidelity simulations have indeed sometimes produced results that disagree with first generation theory, whilst higher fidelity simulations have shown more consistency with basic theory. In short, basic theory and computational simulations represent distinct approaches that are valuable both independently and in combination.

6.2. *Identifying distinct features of PPN-C and PPN-W*

The classification of PPN-W versus PPN-C, respectively, delineates whether the influential binary companion is inside or outside the outer radius of the initial giant star. Which observational consequences manifest from this distinction? In addition to subtle differences that may require simulations to identify, there are some conspicuous distinctions.

PPN-W would show the time variability of a larger binary orbit than PPN-C. Moreover, for PPN-W the jet has a diameter at launch that is much smaller than the orbital separation, so one might expect reflection symmetry to be common as the jet moves around the orbit. In contrast, for PPN-C, the jet cross section is closer to the size of the binary separation itself and less orbital motion of the jet is expected. There is also likely to be more surrounding torus mass for PPN-C than for PPN-W since the former happens inside the circumstellar envelope. This would suggest that more collimation is likely for PPN-C than PPN-W. A PPN-C jet may thus be narrower, possibly with point symmetry rather than reflection symmetry, if the overall jet precesses.

There may also be statistical population differences in duration between PPN-C and PPN-W as they are determined by different accretion processes. PPN-W durations would be determined by how long RLOF accretion occurs before the companion plunges into CEE. Predictions for this duration are not yet clear (MacLeod et al. 2018a). PPN-C would be determined by the time scale for circumbinary material to accrete after CEE but before enough envelope is lost to reduce the mass supply, or the time scale for accretion from a merger to run out of mass.

There may also be some influence of WD nuclear burning that is more common for PPN-C than PPN-W because all PPN-C would have at least 1 WD within its engine. Core X-rays and other signatures of dwarf novae could be more prevalent for PPN-C.

Another distinction is that although RLOF fueled PPN-W can produce a surrounding torus that precedes a jet, only for PPN-W can there also be a torus that follows the jet. This is because the PPN-W happens before CEE, if CEE is to happen. In contrast, the PPN-C would always occur only after all possible tori are produced in the system. This distinction could lead to statistical differences between the timing of jet and tori in the two populations. As emphasized earlier, even magnetized jets require an ambient wind or torus for stable collimation, so some minimum ambient material would be common to both PPN-C and PPN-W.

Finally there may be compositional differences. Since material supplying PPN-W jets comes from farther in the envelope, it may be less C-rich. The jet composition will be dependent on the jet material source, and this also depends on how effectively or ineffectively convective mixing homogenizes the composition.

7. Summary

PPN are more kinematically demanding than PN, and thus place tighter constraints on their mutual origin mechanisms if PN are a time evolved state of PPN. Kinematic constraints for PPN demand close binary interaction, at least as close as RLOF from the primary onto a secondary main-sequence star.

To produce PPN jets, binaries and magnetic fields likely act in symbiosis, with the free energy in orbital motion and accretion used to generate magnetic fields that drive and collimate outflows. The presence of circumstellar tori can in turn collimate and stabilize the magnetic structures, which is likely required to explain observed PPN jets. The classification of PPN jets as either PPN-W or PPN-C can be used to respectively distinguish those for which the binary separation in the engine is wider than, or less than the primary giant envelope radius. Jets produced by RLOF of the giant onto the

secondary are examples of PPN-W, and jets produced after the companion plunges into CEE by a circumbinary disk or merger after the envelope largely unbinds would be PPN-C jets. Examples of both classes were discussed.

There has been significant progress over the past several decades in putting all of the pieces together. This is culminating in increasingly high fidelity simulations. Self-consistently generated magnetic fields, and the associated magnetically mediated jets are now seen to emerge organically in 3-D CE PPN-C simulations. There is open opportunity to achieve the equivalent for PPN-W.

Probing the physics of these simulations and their limitations remains an active effort. Convection is a fundamental feature of observed giants that is absent from most simulations, and presents an important frontier. The extent to which the observed phenomenology depends on initial binary parameters and boundary conditions needs to be explored. Understanding the different classes of PPN that can be produced and their observational signatures will benefit from further collaborations between observers and theorists to converge on specific predictions that can distinguish different mechanisms.

Acknowledgements

References

Alcolea, J., Bujarrabal, V., Sánchez Contreras, C., Neri, R., & Zweigle, J. 2001, A & A, 373, 932
Amiri, N., Vlemmings, W., & van Langevelde, H. J. 2010, A & A, 509, A26
Armitage, P. J., & Livio, M. 2000, ApJ, 532, 540
Balick, B., & Frank, A. 2002, ARAA, 40, 439
Balick, B., Frank, A., & Liu, B. 2020, ApJ, 889, 13
Balick, B., Huarte-Espinosa, M., Frank, A., et al. 2013, ApJ, 772, 20
Balick, B., Preston, H. L., & Icke, V. 1987, AJ, 94, 1641
Blackman, E. G., Carroll-Nellenback, J. J., Frank, A., Huarte-Espinosa, M., & Nordhaus, J. 2013, MNRAS, 436, 904
Blackman, E. G., Frank, A., & Welch, C. 2001, ApJ, 546, 288
Blackman, E. G., & Lucchini, S. 2014, MNRAS, 440, L16
Blackman, E. G., & Nauman, F. 2015, Journal of Plasma Physics, 81, 395810505
Blackman, E. G., & Pessah, M. E. 2009, ApJl, 704, L113
Blandford, R. D., & Payne, D. G. 1982, MNRAS, 199, 883
Boffin, H. M. J., & Jones, D. 2019, The Importance of Binaries in the Formation and Evolution of Planetary Nebulae (Springer), doi:10.1007/978-3-030-25059-1
Bollen, D., Kamath, D., Van Winckel, H., De Marco, O., & Wardle, M. 2021, MNRAS, 502, 445
Bond, H. 2000, in Encyclopedia of Astronomy and Astrophysics, ed. P. Murdin (IOP), 2382
Borkowski, K. J., Blondin, J. M., & Harrington, J. P. 1997, ApJL, 482, L97
Bryce, M., López, J. A., Holloway, A. J., & Meaburn, J. 1997, ApJL, 487, L161
Bujarrabal, V., Castro-Carrizo, A., Alcolea, J., & Sánchez Contreras, C. 2001, A. & Ap., 377, 868
Chamandy, L., Blackman, E. G., Frank, A., Carroll-Nellenback, J., & Tu, Y. 2020, MNRAS, 495, 4028
Chamandy, L., Blackman, E. G., Frank, A., et al. 2019a, MNRAS, 490, 3727
Chamandy, L., Blackman, E. G., Nordhaus, J., & Wilson, E. 2021, MNRAS, 502, L110
Chamandy, L., Tu, Y., Blackman, E. G., et al. 2019b, MNRAS, 486, 1070

Chamandy, L., Frank, A., Blackman, E. G., et al. 2018, MNRAS, 480, 1898

Chen, Z., Blackman, E. G., Nordhaus, J., Frank, A., & Carroll-Nellenback, J. 2018, MNRAS, 473, 747

Chen, Z., Frank, A., Blackman, E. G., Nordhaus, J., & Carroll-Nellenback, J. 2017, MNRAS, 468, 4465

Chevalier, R. A. 2012, ApJL, 752, L2

Chevalier, R. A., & Luo, D. 1994, ApJ, 421, 225

Chong, S.-N., Imai, H., & Diamond, P. J. 2015, ApJ, 805, 53

Ciardullo, R., Bond, H. E., Sipior, M. S., et al. 1999, AJ, 118, 488

Ciolfi, R. 2020, General Relativity and Gravitation, 52, 59

Cohen, M., Van Winckel, H., Bond, H. E., & Gull, T. R. 2004, AJ, 127, 2362

Cohen, N. L., Hohfeld, R. G., Gorenstein, M. V., Pottash, R. I., & Willson, R. F. 1981, A & A, 95, 386

Corradi, R. L. M. 2012, Memorie della Societa Astronomica Italiana, 83, 811

Corradi, R. L. M., Livio, M., Balick, B., Munari, U., & Schwarz, H. E. 2001, ApJ, 553, 211

Corradi, R. L. M., Sabin, L., Miszalski, B., et al. 2011, MNRAS, 410, 1349

De Marco, O., & Soker, N. 2011, PASP, 123, 402

Decin, L., Montargès, M., Richards, A. M. S., et al. 2020, Science, 369, 1497

Diamond, P. J., & Nyman, L. Å. 1988, in The Impact of VLBI on Astrophysics and Geophysics, ed. M. J. Reid & J. M. Moran, Vol. 129, 249

Dodson, R., Rioja, M., Bujarrabal, V., et al. 2018, MNRAS, 476, 520

Doyle, S., Balick, B., Corradi, R. L. M., & Schwarz, H. E. 2000, AJ, 119, 1339

Edgar, R. G., Nordhaus, J., Blackman, E. G., & Frank, A. 2008, ApJL, 675, L101

Etoka, S., & Diamond, P. 2004, MNRAS, 348, 34

Feibelman, W. A. 1985, AJ, 90, 2550

Gan, Z., Li, H., Li, S., & Yuan, F. 2017, ApJ, 839, 14

Garcia-Segura, G. 1997, ApJL, 489, L189

García-Segura, G., Langer, N., Różyczka, M., & Franco, J. 1999, ApJ, 517, 767

García-Segura, G., López, J. A., & Franco, J. 2005, ApJ, 618, 919

García-Segura, G., Ricker, P. M., & Taam, R. E. 2018, ApJ, 860, 19

García-Segura, G., Taam, R. E., & Ricker, P. M. 2020, ApJ, 893, 150

—. 2021, ApJ, 914, 111

Gieseking, F., Becker, I., & Solf, J. 1985, ApJL, 295, L17

Glanz, H., & Perets, H. B. 2018, ArXiv e-prints, arXiv:1801.08130

Herpin, F., Baudry, A., Thum, C., Morris, D., & Wiesemeyer, H. 2006, A & A, 450, 667

Hillwig, T. C., Jones, D., De Marco, O., et al. 2016, ApJ, 832, 125

Huarte-Espinosa, M., Carroll-Nellenback, J., Nordhaus, J., Frank, A., & Blackman, E. G. 2013, MNRAS, 433, 295

Huggins, P. J. 2007, ApJ, 663, 342

Huggins, P. J. 2012, in American Astronomical Society Meeting Abstracts, Vol. 219, American Astronomical Society Meeting Abstracts #219, 239.01

Iaconi, R., De Marco, O., Passy, J.-C., & Staff, J. 2018, MNRAS, 477, 2349

Iaconi, R., Maeda, K., De Marco, O., Nozawa, T., & Reichardt, T. 2019, MNRAS, 489, 3334

Iaconi, R., Maeda, K., Nozawa, T., De Marco, O., & Reichardt, T. 2020, arXiv e-prints, arXiv:2003.06151

Iaconi, R., Reichardt, T., Staff, J., et al. 2017, MNRAS, 464, 4028

Iben, Jr., I., & Livio, M. 1993, PASP, 105, 1373

Imai, H., Nakashima, J.-i., Diamond, P. J., Miyazaki, A., & Deguchi, S. 2005, ApJL, 622, L125

Imai, H., Sasao, T., Obara, K., Omodaka, T., & Diamond, P. J. 2002, in Cosmic Masers: From Proto-Stars to Black Holes, ed. V. Migenes & M. J. Reid, Vol. 206, 80

Ivanova, N. 2011, ApJ, 730, 76

—. 2018, ApJl, 858, L24

Ivanova, N., Justham, S., Avendano Nandez, J. L., & Lombardi, J. C. 2013a, Science, 339, 433

Ivanova, N., Justham, S., & Podsiadlowski, P. 2015, MNRAS, 447, 2181

Ivanova, N., & Nandez, J. L. A. 2016, MNRAS, 462, 362

Ivanova, N., Justham, S., Chen, X., et al. 2013b, A. & Ap.r, 21, 59

Jacoby, G. H., Hillwig, T. C., Jones, D., et al. 2021, MNRAS, 506, 5223

Jones, D. 2020, Galaxies, 8, 28

Jura, M., Turner, J., Balm, & S. P. 1997, ApJ, 474, 741

Kastner, J. H., Weintraub, D. A., Merrill, K. M., & Gatley, I. 1998, AJ, 116, 1412

Kathirgamaraju, A., Tchekhovskoy, A., Giannios, D., & Barniol Duran, R. 2019, MNRAS, 484, L98

Kemball, A. J., & Diamond, P. J. 1997, ApJL, 481, L111

Kemball, A. J., Diamond, P. J., Gonidakis, I., et al. 2009, ApJ, 698, 1721

Khouri, T., Vlemmings, W. H. T., Tafoya, D., et al. 2021, Nature Astronomy, arXiv:2112.09689

Kim, H., Trejo, A., Liu, S.-Y., et al. 2017, Nature Astronomy, 1, 0060

Kwok, S., Purton, C. R., & Fitzgerald, P. M. 1978, ApJL, 219, L125

Leone, F., Corradi, R. L. M., Martínez González, M. J., Asensio Ramos, A., & Manso Sainz, R. 2014, A & A, 563, A43

Lopez, J. A., Meaburn, J., & Palmer, J. W. 1993, ApJL, 415, L135

López-Cámara, D., De Colle, F., & Moreno Méndez, E. 2019, MNRAS, 482, 3646

Lopez-Camara, D., De Colle, F., Moreno Mendez, E., Shiber, S., & Iaconi, R. 2021, arXiv e-prints, arXiv:2110.02227

Lykou, F., Chesneau, O., Zijlstra, A. A., et al. 2011, A & A, 527, A105

Lynden-Bell, D. 1996, MNRAS, 279, 389

—. 2003, MNRAS, 341, 1360

MacLeod, M., Antoni, A., Murguia-Berthier, A., Macias, P., & Ramirez-Ruiz, E. 2017, ApJ, 838, 56

MacLeod, M., Ostriker, E. C., & Stone, J. M. 2018a, ArXiv e-prints, arXiv:1808.05950

—. 2018b, ApJ, 863, 5

MacLeod, M., & Ramirez-Ruiz, E. 2015a, ApJ, 803, 41

—. 2015b, ApJl, 798, L19

Madappatt, N., De Marco, O., & Villaver, E. 2016, MNRAS, 463, 1040

Matt, S., Frank, A., & Blackman, E. G. 2006, ApJL, 647, L45

Mauron, N., & Huggins, P. J. 2006, A & A, 452, 257

Meyer, F., & Meyer-Hofmeister, E. 1983, A & A, 121, 29

Miranda, L. F., & Solf, J. 1990, Ap& SS, 171, 227

Miszalski, B., Acker, A., Moffat, A. F. J., Parker, Q. A., & Udalski, A. 2009, A & A, 496, 813

Moe, M., & De Marco, O. 2006, ApJ, 650, 916

Mohamed, S., & Podsiadlowski, P. 2012, Baltic Astronomy, 21, 88

Moreno Méndez, E., López-Cámara, D., & De Colle, F. 2017, MNRAS, 470, 2929

Murakawa, K., & Izumiura, H. 2012, A & A, 544, A58

Nordhaus, J., & Blackman, E. G. 2006, MNRAS, 370, 2004

Nordhaus, J., Blackman, E. G., & Frank, A. 2007, MNRAS, 376, 599

O'Connor, J. A., Redman, M. P., Holloway, A. J., et al. 2000, ApJ, 531, 336

Ohlmann, S. T., Röpke, F. K., Pakmor, R., & Springel, V. 2016a, ApJl, 816, L9

—. 2017, A. & Ap., 599, A5

Ohlmann, S. T., Röpke, F. K., Pakmor, R., Springel, V., & Müller, E. 2016b, MNRAS, 462, L121

Olofsson, H., Vlemmings, W., Maercker, M., et al. 2015, in Astronomical Society of the Pacific Conference Series, Vol. 499, Revolution in Astronomy with ALMA: The Third Year, ed. D. Iono, K. Tatematsu, A. Wootten, & L. Testi, 319

Ondratschek, P. A., Roepke, F. K., Schneider, F. R. N., et al. 2021, arXiv e-prints, arXiv:2110.13177

Paczynski, B. 1976, in IAU Symposium, Vol. 73, Structure and Evolution of Close Binary Systems, ed. P. Eggleton, S. Mitton, & J. Whelan, 75

Papish, O., Soker, N., & Bukay, I. 2015, MNRAS, 449, 288

Pascoli, G. 1997, ApJ, 489, 946

Pelletier, G., & Pudritz, R. E. 1992, ApJ, 394, 117

Perez-Sanchez, A. F., Vlemmings, W. H. T., Tafoya, D., & Chapman, J. M. 2013, MNRAS, 436, L79

Postnov, K. A., & Yungelson, L. R. 2014, Living Reviews in Relativity, 17, 3

Raghavan, D., McAlister, H. A., Henry, T. J., et al. 2010, ApJS, 190, 1

Reichardt, T. A., De Marco, O., Iaconi, R., Tout, C. A., & Price, D. J. 2019, MNRAS, 484, 631

Reyes-Ruiz, M., & López, J. A. 1999, ApJ, 524, 952

Ricker, P. M., & Taam, R. E. 2012, ApJ, 746, 74

Riera, A., Velázquez, P. F., Raga, A. C., Estalella, R., & Castrillón, A. 2014, A & A, 561, A145

Ritter, H. 1988, A & A, 202, 93

Ruiz, M., Tsokaros, A., & Shapiro, S. L. 2021, Phys. Rev. D., 104, 124049

Sabin, L., Hull, C. L. H., Plambeck, R. L., et al. 2015, MNRAS, 449, 2368

Sahai, R., Sugerman, B. E. K., & Hinkle, K. 2009, ApJ, 699, 1015

Sahai, R., & Trauger, J. T. 1998, AJ, 116, 1357

Sahai, R., Vlemmings, W. H. T., Gledhill, T., et al. 2017, ApJl, 835, L13

Sánchez Contreras, C., Alcolea, J., Bujarrabal, V., et al. 2018, A & A, 618, A164

Sánchez Contreras, C., Gil de Paz, A., & Sahai, R. 2004, ApJ, 616, 519

Shiber, S., Iaconi, R., De Marco, O., & Soker, N. 2019, MNRAS, 488, 5615

Shiber, S., Kashi, A., & Soker, N. 2017, MNRAS, 465, L54

Shiber, S., & Soker, N. 2018, MNRAS, arXiv:1706.00398

Soker, N. 1994, MNRAS, 270, 774

—. 1996, ApJ, 469, 734

—. 1997, ApJS, 112, 487

—. 2002, ApJ, 568, 726

—. 2004, New Astron., 9, 399

—. 2006, PASP, 118, 260

—. 2015, ApJ, 800, 114

—. 2016, New Astron. Revs, 75, 1

Soker, N., & Livio, M. 1989, ApJ, 339, 268

—. 1994, ApJ, 421, 219

Soker, N., & Rappaport, S. 2000, ApJ, 538, 241

—. 2001, ApJ, 557, 256

Staff, J. E., De Marco, O., Macdonald, D., et al. 2016a, MNRAS, 455, 3511

Staff, J. E., De Marco, O., Wood, P., Galaviz, P., & Passy, J.-C. 2016b, MNRAS, 458, 832

Taam, R. E., & Sandquist, E. L. 2000, ARAA, 38, 113

Tafoya, D., Imai, H., Gómez, J. F., et al. 2020, ApJL, 890, L14

Tocknell, J., De Marco, O., & Wardle, M. 2014, MNRAS, 439, 2014

Tout, C. A., & Regos, E. 2003, in Astronomical Society of the Pacific Conference Series, Vol. 293, 3D Stellar Evolution, ed. S. Turcotte, S. C. Keller, & R. M. Cavallo, 100

Uzdensky, D. A., & MacFadyen, A. I. 2006, ApJ, 647, 1192

Vlemmings, W. H. T., Diamond, P. J., & Imai, H. 2006, Nature, 440, 58

Wilson, E. C., & Nordhaus, J. 2019, MNRAS, 485, 4492

Witt, A. N., Vijh, U. P., Hobbs, L. M., et al. 2009, ApJ, 693, 1946

Zou, Y., Frank, A., Chen, Z., et al. 2020, MNRAS, 497, 2855